Propagation, cavity, and Doppler-broadening effects in the collective atomic recoil laser

R. Bonifacio and G. R. M. Robb*
Dipartimento di Fisica, Universita degli Studi, INFN and INFM, Sezione di Milano, via Celoria 16, I-20133 Milano, Italy

B. W. J. McNeil
Department of Physics and Applied Physics, University of Strathclyde, Glasgow, G4 0NG, Scotland
(Received 23 December 1996)

Using a completely semiclassical approach we extend a previous theory of the collective atomic recoil laser to include propagation effects with and without a ring cavity, and to take into account the effects of Doppler broadening. For cold atoms, we determine a mean-field condition under which propagation effects are negligible, and find different dynamical regimes that we classify as ''good'' and ''bad'' cavity limits. We obtain the results of a previous single-mode theory only in the good cavity limit. In the bad cavity limit or in free space collective superradiant behavior dominates. For warm beams, where Doppler-broadening effects are important, a noncollective Raman gain mechanism dominates in general, as recently observed experimentally. The effects of particle trapping in the ponderomotive potential and radiation pressure have been described. [S1050-2947(97)04407-7]

PACS number(s): 42.55.−f, 42.50.−p, 32.80.Pj

I. INTRODUCTION

The collective atomic recoil laser (CARL) consists of a beam of two-level noninverted particles (e.g., atoms, ions, or electrons, generically called atoms) coherently driven by a quasiresonant counterpropagating field [1]. The CARL mechanism is the collective regime of recoil induced gain phenomena which have been the subject of recent experimental investigations [2–5]. This system can give rise to collective coherent Compton backscattering due to self-bunching of the atoms via an instability very similar to that which occurs in the high-gain Compton free-electron laser (FEL), with the dispersive part of the atomic polarization playing a role analogous to the FEL wiggler magnetic field. The spontaneous grating formed by the atomic bunching has been demonstrated experimentally by Bragg scattering [4]. The source of the radiation is both the internal degrees of freedom of the atoms, similar to a conventional atomic laser but without population inversion, and the translational motion of the atoms similar to the FEL. To date, theoretical treatments of CARL have considered only a single mode and have neglected propagation effects. The effect of a cavity was treated phenomenologically as a loss term. In this paper, we give a first principle treatment of propagation effects and the cavity is described in an exact manner by imposing proper boundary conditions on the field. The one-mode description of previous papers is recovered here in the so-called mean-field limit specifying the limit of validity in which propagation effects can be neglected.

In Sec. II of this paper we derive a system of equations which describe CARL from a completely semiclassical approach by generalizing the so-called Maxwell-Bloch equations [6] and using a Hamiltonian of the system. In Sec. III we extend the CARL model of previous papers [1] to include the effects of the relative propagation of the scattered electromagnetic field with respect to the atoms when the atomic sample is in free space. It was found that a superradiant solitonlike pulse of radiation was produced. In Sec. IV we extend the analysis of propagation effects to cases where the atomic sample is enclosed in a ring cavity. A mean-field condition, which allows the neglect of propagation effects, is derived and the dynamics of the CARL interaction are described by a damping parameter K'. When $K' \ll 1$, the cavity is said to be ''good,'' and the field evolution is identical to that in a Compton FEL neglecting slippage. When $K' \geqslant 1$, the cavity is said to be ''bad,'' and a super-radiant pulse of radiation is produced. In Sec. V we investigate how a distribution of atomic momenta (Doppler broadening) affects the evolution of the probe field. It is shown that the effect of a sufficiently large Doppler broadening is to reduce the atomic bunching and so the amplitude of the radiation emitted. This warm beam regime is characterized by noncollective effects giving rise to a Raman gain mechanism. For long-time scales it is shown that the steady state of this regime may be unstable due to atomic trapping leading to a synchrotron instability similar to that of the FEL. Finally in Sec. VI we investigate the effects of the radiation pressure exerted by the pump field upon the CARL evolution. It is shown that in the cold beam limit the radiation pressure decreases the peak intensity of the emitted radiation and also introduces a frequency chirp to it. In the warm beam limit the effects are similarly to reduce the peak intensity of the emitted radiation and also to introduce an instability of the steady-state gain, the onset of which has been observed experimentally.

II. DERIVATION OF THE CARL EQUATIONS

In previous papers [1] the CARL equations have been derived starting from a quantum-mechanical Hamiltonian which described the interaction of two counterpropagating single-mode fields with a two-level atomic system. This fundamental approach is unnecessary in the semiclassical limit

*Present address: Department of Physics and Applied Physics, University of Strathclyde, Glasgow, G4 0NG, Scotland.

which was used and has the drawback of not describing the effects of propagation. We now derive the CARL equations using a semiclassical approach from the outset allowing propagation effects to be investigated.

Let us assume an electric field linearly polarized in $\hat{\mathbf{x}}$ with an amplitude of the form

$$\mathbf{E}(z,t)=[A_1(z,t)e^{ik(z-ct)}+A_2e^{-ik(z+ct)}+\text{c.c.}]\hat{\mathbf{x}}, \quad (1)$$

$\mathbf{E}(z,t)$ represents two counterpropagating plane waves in $\pm\hat{\mathbf{z}}$. We define the strong pump field A_2 as a real constant and the weak counterpropagating probe field $A_1(z,t)$ as a complex variable. For each atom this electric field will create a dipole moment $\mathbf{d}$ and the interaction of the dipole with the electric field is described by the classical Hamiltonian

$$H=\sum_{j=1}^{N}\left(\frac{p_j^2}{2M}-\mathbf{d}_j\cdot\mathbf{E}(z_j,t)\right),$$

where M is the atomic mass, the canonical position and momentum are z_j and p_j, respectively, and N is the total number of atoms. The z component of the force on the jth atom is then given by

$$\dot{p}_j=-\frac{\partial H}{\partial z_j}=\mathbf{d}_j\cdot\frac{\partial\mathbf{E}(z_j,t)}{\partial z_j}. \quad (2)$$

We define $\mathbf{d}_j$ to be of the form

$$\mathbf{d}_j=\mu(S_je^{-i(kz_j+\omega t)}+\text{c.c.})\hat{\mathbf{x}}, \quad (3)$$

where μ and S_j are the atomic dipole matrix element and the amplitude of the dipole moment of the jth atom, respectively, the precise form of which will be discussed in terms of the Bloch equations [6] shortly. Substituting Eqs. (1) and (3) into Eq. (2) we obtain

$$\dot{p}_j=ik\mu(A_1S_j^*e^{i\theta_j}-A_2S_j^*-\text{c.c.}), \quad (4)$$

where $\theta_j=2kz_j$ and rapidly oscillating terms varying as $e^{\pm i2\omega t}$ have been neglected.

We now calculate the dipole moment amplitude S_j using the Bloch equations in the steady-state adiabatic approximation as in [8], i.e., for times longer than γ^{-1}, where γ is the natural linewidth of the transition. One obtains

$$\text{Re}(S)=-S_0, \quad (5)$$

$$\text{Im}(S)=-\frac{\gamma}{\Delta}\text{Re}(S), \quad (6)$$

where

$$S_0=\frac{\Omega\Delta}{2(\Delta^2+\gamma^2+\Omega^2)} \quad (7)$$

and

$$\Omega=\frac{2\mu}{\hbar}A_2 \quad (8)$$

is the Rabi frequency of the pump field. These equations can be derived easily, assuming that the atoms evolve only under the action of the pump field A_2, which dominates the probe field A_1, and neglecting the recoil frequency shift $k\dot{z}_j$ with respect to the pump detuning $\Delta=\omega-\omega_0$, where ω_0 is the atomic transition frequency.

As is usual $\text{Im}(S)$ describes absorbtion and, as will be seen, results in a force due to radiation pressure, whereas $\text{Re}(S)$ describes dispersion and will be seen to result in a ponderomotive force which gives rise to spatial bunching of the atoms. In order to minimize the radiation pressure we choose

$$\Delta\gg\gamma, \quad (9)$$

so that, from Eq. (6), we have $\text{Im}(S)\ll\text{Re}(S)$, i.e., the system is essentially dispersive. In this case, one can neglect γ^2 in the denominator of $\text{Re}(S)$, which can be maximized by assuming $\Delta\approx\Omega\gg\gamma$, so that

$$S_0\approx\tfrac{1}{4}. \quad (10)$$

Under condition (9) we can neglect $\text{Im}(S)$ in Eq. (4) to obtain

$$\dot{\theta}_j=\frac{2k}{M}p_j, \quad (11)$$

$$\dot{p}_j=-ik\mu S_0(A_1e^{i\theta_j}-\text{c.c.})-\frac{\hbar k\gamma\Omega^2}{2(\Delta^2+\Omega^2)}, \quad (12)$$

where S_0, given by Eq. (7), contains the dependence of the recoil on the pump field amplitude and pump detuning. The first term of Eq. (12) is the ponderomotive force which produces the spatial bunching of the atoms, and the second term is the force due to the radiation pressure of the pump. If the probe field A_1 is a given constant and radiation pressure is neglected, these equations represent a system of decoupled pendula.

The probe field A_1 will evolve self-consistently under the presence of the coherent polarization of the atoms so that amplification may occur. To describe this process we write the Maxwell wave equation for an electric field in the presence of a polarization $\mathbf{P}$:

$$\frac{\partial^2\mathbf{E}}{\partial t^2}-c^2\nabla^2\mathbf{E}=-\frac{1}{\epsilon_0}\frac{\partial^2\mathbf{P}}{\partial t^2}. \quad (13)$$

Substituting for $\mathbf{E}(z,t)$ from Eq. (1), and performing the slowly varying envelope approximation (SVEA) for A_1 (remembering that A_2 is a constant), one obtains

$$\left(\frac{\partial A_1}{\partial t}+c\frac{\partial A_1}{\partial z}\right)=i\frac{\omega}{2\epsilon_0}Pe^{-i(kz-\omega t)}, \quad (14)$$

where $P=\mathbf{P}\cdot\hat{\mathbf{x}}$ and in the spirit of SVEA, we have made the approximation

$$\frac{\partial^2P}{\partial t^2}\approx-\omega^2P.$$

Assuming N atoms at positions $\mathbf{r}_j$, then

$$P=\hat{\mathbf{x}}\cdot\sum_{j=1}^{N}\mathbf{d}_j\delta(\mathbf{r}-\mathbf{r}_j).$$

Substituting for $\mathbf{d}_j$ using Eq. (3), performing a spatial average over volume V, and neglecting rapidly oscillating terms, one obtains

$$\frac{\partial A_1}{\partial t}+c\frac{\partial A_1}{\partial z}=\frac{i\omega\mu n}{2\epsilon_0}\langle S_j e^{-i\theta}\rangle=\frac{-i\omega\mu n S_0}{2\epsilon_0}\langle e^{-i\theta}\rangle, \tag{15}$$

where $n=N/V$ is the atomic density, $\langle\cdots\rangle=(1/N)\Sigma_{j=1}^{N}\ldots$. Under the conditions described above, which mimimize the radiation pressure force, and again assuming $A_2\gg|A_1|$, we find that $|\mathrm{Re}(S)|\gg|\mathrm{Im}(S)|$ and we have replaced S_j with the j-independent real part $\mathrm{Re}(S)=-S_0$ in the second equality. We define

$$b=\langle e^{-i\theta}\rangle \tag{16}$$

as the bunching factor. Equations (11), (12), and (15) now form a self-consistent system describing atomic phase, momentum, and field evolution.

We now introduce the universal scaling for these equations. Let us define the fundamental dimensionless CARL parameter as

$$\rho=\left(\frac{\omega\mu^2 n S_0^2}{2\epsilon_0\hbar\omega_r^2}\right)^{1/3}, \tag{17}$$

where $\omega_r=2\hbar k^2/M$ is the one-photon recoil frequency shift. Defining the dimensionless quantities

$$\overline{t}=\omega_r\rho t,\quad \overline{z}=\frac{\omega_r\rho}{c}z,\quad A=iA_1\left(\frac{2\epsilon_0}{\hbar\omega n\rho}\right)^{1/2}, \tag{18}$$

$$\overline{p}=\frac{(p-Mv_{ph})}{\hbar k\rho}, \tag{19}$$

we obtain our working system of equations

$$\frac{\partial\theta_j}{\partial\overline{t}}=\overline{p_j}, \tag{20}$$

$$\frac{\partial\overline{p_j}}{\partial\overline{t}}=-(Ae^{i\theta_j}+\mathrm{c.c.})-\frac{\Omega^2\gamma}{2(\Delta^2+\Omega^2)\omega_r\rho^2}, \tag{21}$$

$$\frac{\partial A}{\partial\overline{t}}+\frac{\partial A}{\partial\overline{z}}=\langle e^{-i\theta}\rangle, \tag{22}$$

where $j=1,\ldots,N$, and

$$v_{ph}=\left(\frac{\omega_1-\omega_2}{\omega_1+\omega_2}\right)c \tag{23}$$

is the phase velocity of the ponderomotive potential formed by the probe field and the polarization induced by the pump, if one allows the probe and the pump to have slightly different frequencies ω_1 and ω_2, respectively. In such a case the atomic phase, with respect to the potential, becomes $\theta_j=(k_1+k_2)z_j-(\omega_1-\omega_2)t$. As a consequence, according to Eq. (11), the scaled momentum $\overline{p_j}$ is given by Eq. (19).

The radiation pressure term has been obtained from Eq. (12) using Eqs. (6) and (8), assuming condition (9) is satisfied. The radiation pressure can be neglected for $(\Omega^2\gamma)/[2(\Delta^2+\Omega^2)\omega_r\rho^2]\ll 1$ and sufficiently short times, so that the momentum change due to this pressure is negligible. In this limit, Eqs. (20)–(22) reduce to a set which have no free parameters and are formally identical to the one-dimensional model of the FEL [9].

Note that as in FEL theory

$$\rho|A|^2=\frac{2\epsilon_0|A_1|^2}{\hbar\omega n}=\frac{\epsilon_0E^2}{\hbar\omega n}=\frac{|a|^2}{N} \tag{24}$$

is the efficiency. In the last equality $|a|^2$ is the classical analogue of the photon number. The relation between a and A_1 is $|A_1|=|a|\sqrt{\hbar\omega/(2\epsilon_0V)}$ due to Eq. (1): $\epsilon_0E^2=2\epsilon_0|A_1|^2=(\hbar\omega|a|^2)/V$. Hence, $\rho|A|^2$ is interpreted as the number of photons emitted per atom. In Sec. III we investigate the solutions to Eqs. (20)–(22), both in free space and in a ring cavity.

III. PROPAGATION EFFECTS IN FREE SPACE

In this section we investigate the effect of the propagation of the probe field with respect to the atoms. We neglect the effect of radiation pressure, so that the equations to be solved are

$$\frac{\partial\theta_j}{\partial\overline{t}}=\overline{p_j}, \tag{25}$$

$$\frac{\partial\overline{p_j}}{\partial\overline{t}}=-(Ae^{i\theta_j}+\mathrm{c.c.}), \tag{26}$$

$$\frac{\partial A}{\partial\overline{t}}+\frac{\partial A}{\partial\overline{z}}=\langle e^{-i\theta}\rangle, \tag{27}$$

where $j=1,\ldots,N$. For now we assume that the atoms are cold. This assumption corresponds to the initial conditions $\overline{p_j}=\delta$, a constant detuning for all atoms, where

$$\delta=\frac{M(v(\overline{t}=0)-v_{ph})}{\hbar k\rho}\approx\frac{\omega_2-\omega_1}{\omega_r\rho}. \tag{28}$$

$v=\dot{z}$ is the translational velocity of the atoms and it has been assumed that the atoms are stationary at the beginning of the interaction, i.e., $v(\overline{t}=0)=0$. δ is, therefore, the scaled frequency detuning between the pump and probe fields. Using the following ansatz on the field and atomic variables [9]

$$\theta_j=\theta_{1j}(y),\quad p_j=\sqrt{\overline{z}}\,p_{1j}(y),\quad A=\overline{z}\,A_1(y) \tag{29}$$

where $y=(\overline{t}-\overline{z})\sqrt{\overline{z}}$, the system of partial differential equations (25)–(27) can be recast as a set of *ordinary* differential equations

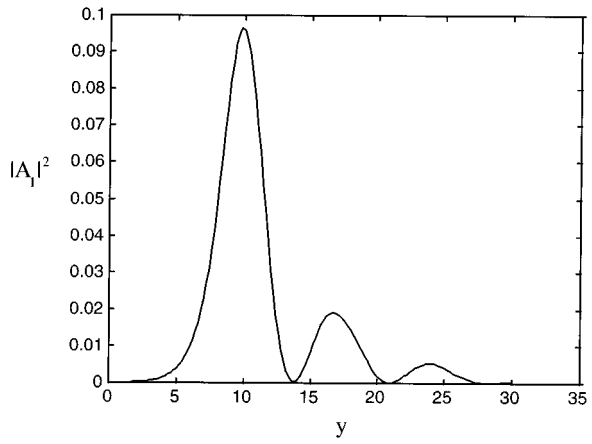

FIG. 1. Intensity of self-similar superradiant pulse $|A_1|^2$ in adimensional units as a function of $y=(t-z)\sqrt{z}$, when $\delta=0$ and $A_1(y=0)=0.01$.

$$\frac{d\theta_{1j}}{dy}=p_{1j}, \tag{30}$$

$$\frac{dp_{1j}}{dy}=-(A_1 e^{i\theta_{1j}}+\text{c.c.}), \tag{31}$$

$$\frac{y}{2}\frac{dA_1}{dy}+A_1=b. \tag{32}$$

Equations (30)–(32) have a self-similar solitonlike solution which depends only on y [9] (see Fig. 1). Hence, from Eq. (29) $|A|^2\propto\overline{z^2}\propto\rho^2 z^2$, so using the definition of ρ, Eqs. (17) and (24), we obtain the scaling $\epsilon_0|E|^2\propto n^2 z^2$, characteristic of a superradiant process. Hence, the pulse amplitude increases linearly with the distance $\overline{z}$ and the time duration, or width, of the pulse varies as $1/\sqrt{\overline{z}}$. This is a collective gain mechanism which leads to the generation of a pulse which increases in amplitude and decreases in width as it propagates through the sample. For a sufficiently long sample a narrow high-intensity spike of radiation is formed analogous to superradiance in the high-gain FEL [9]. The pulse shape of Fig. 1 can be approximated by a hyperbolic secant function [10], followed by nonlinear ''ringing'' which is very similar to the radiation pulse shape which occurs in superradiance or superfluorescence from atomic two-level systems [7].

IV. PROPAGATION EFFECTS IN A RING CAVITY

In a ring cavity (see Fig. 2), the boundary condition for the electric-field is $E(0,t)=\sqrt{T}E_I(t)+RE(L,t-\tau)$, where E_I is the value of the electric field input to the cavity, L is the sample length, $\tau=(\Lambda-L)/c$, Λ is the cavity length, and $T=1-R$ is the transmission coefficient of the mirrors. Rewriting the electric field in terms of a slowly varying envelope $E(z,t)=\overline{E}(z,t)e^{ik(z-ct)}$ and with the same normalization as Eqs. (25)–(27), then

$$A(0,\overline{t})=\sqrt{T}A_I+RA(\overline{L},\overline{t}-\overline{\tau}), \tag{33}$$

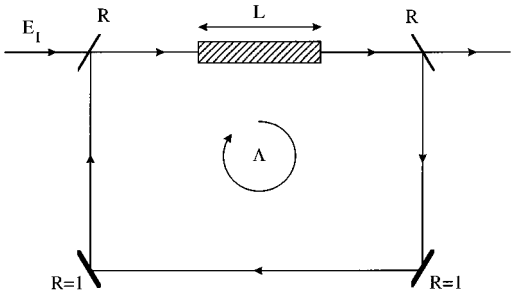

FIG. 2. Schematic diagram of a ring cavity. The counterpropagating pump field is not shown.

where $\overline{L}=L/l_c$, $\overline{\Lambda}=\Lambda/l_c$, $\overline{\tau}=\overline{\Lambda}-\overline{L}$, $l_c=c/\omega_r\rho$ is the cooperation length of the system and we have assumed that $k\Lambda=2n\pi$, where n is an integer, so that the wave number k coincides with that of a cavity mode.

If we introduce the variable $\overline{A}$ as

$$A(\overline{z},\overline{t})=\overline{A}(\overline{z},\overline{t})e^{K\overline{z}}+\frac{A_I}{\sqrt{T}} \tag{34}$$

and set $K=\ln(1/R)/\overline{L}$, then the boundary condition (33) becomes

$$\overline{A}(0,\overline{t})=\overline{A}(\overline{L},\overline{t}-\overline{\tau}). \tag{35}$$

Introducing the new independent variables

$$z'=\overline{z} \quad \text{and} \quad t'=\overline{t}+\frac{\overline{\tau z}}{\overline{L}}, \tag{36}$$

the retardation factor $\overline{t}-\overline{\tau}$ can be removed from the boundary condition, resulting in

$$\overline{A}(0,t')=\overline{A}(\overline{L},t'), \tag{37}$$

so that $\overline{A}$ satisfies periodic boundary conditions. Using Eqs. (34) and (36), the field evolution equation (27) can be written as

$$\frac{\partial\overline{A}}{\partial t'}+\frac{\overline{L}}{\overline{\Lambda}}\frac{\partial\overline{A}}{\partial z'}+\frac{\overline{L}}{\overline{\Lambda}}K\overline{A}=b\frac{\overline{L}}{\overline{\Lambda}}e^{-Kz'}. \tag{38}$$

The effect of the change of variables (36) is, therefore, to move to a coordinate system where the velocity of the radiation field envelope is $(L/\Lambda)c<c$, therefore reducing the relative slippage of the radiation with respect to the almost stationary atoms. Note that Eq. (36) also implies that if $A\propto e^{Ct'}$, where C is a real positive constant, then the field amplitude will grow exponentially in time and space.

The factor $\overline{L}/\overline{\Lambda}$ in front of b in Eq. (38) can be removed by replacing ρ in the definitions of $\overline{t}$, $\overline{z}$, and p_j by ρ', where

$$\rho'=\rho\left(\frac{\overline{L}}{\overline{\Lambda}}\right)^{1/3}\propto\left(n\frac{L}{\Lambda}\right)^{1/3}\propto(n')^{1/3},$$

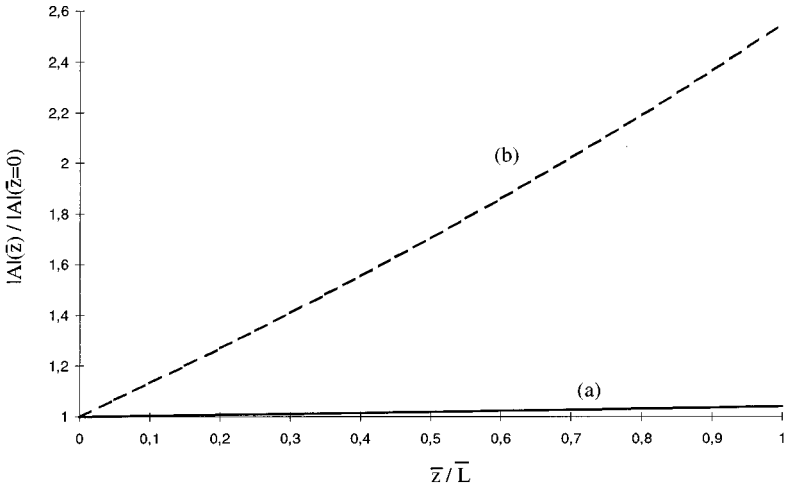

FIG. 3. Spatial evolution of the normalized field amplitude $|A(\overline{z})|/|A(\overline{z}=0|)/$ as a function of $\overline{z/L}$ for $\overline{L}=0.05$, $T=0.01$, $|A_I|=0.001$, when (a) spatial derivative may be neglected: $\overline{\Lambda}=0.1$ when $\overline{t}=10$, (b) spatial derivative may not be neglected: $\overline{\Lambda}=5$ and $\overline{t}=30$. These plots were obtained from a numerical solution of Eqs. (25) and (27) with the boundary condition (33).

where $n'=N/V_c$ is the number of atoms per unit *cavity* volume. We denote the rescaled variables as $\overline{t'}$, $\overline{z'}$, and p_j', respectively. The rescaled field variable $\overline{A'}$ is defined by replacing ρ and n by ρ' and n', respectively, in the definition of A (24).

After this rescaling, Eq. (38) can be written as

$$\frac{\partial\overline{A'}}{\partial\overline{t'}}+\frac{\overline{L}}{\overline{\Lambda}}\frac{\partial\overline{A'}}{\partial\overline{z'}}+K'\overline{A'}=be^{-K'\overline{z'}\,\overline{\Lambda}/\overline{L}}, \tag{39}$$

where the scaled damping parameter is

$$K'=(\overline{\Lambda}\sqrt{\overline{L}})^{-2/3}\ln(1/R). \tag{40}$$

From now on, we impose the condition that $R\approx 1$, which allows us to assume that the exponential term on the right-hand side (RHS) of Eq. (39) has a value ≈ 1.

The mean-field approximation

We now consider the mean-field approximation, which consists of assuming that the electromagnetic field is almost uniform across the sample. From an inspection of Eq. (39), the spatial derivative term can be neglected when $\overline{z'}\,\overline{\Lambda}/\overline{L}\ll 1$. Recalling that $\overline{z'}=\overline{z}(\overline{L}/\overline{\Lambda})^{1/3}$, and setting $\overline{z}$ to its maximum value $\overline{z}=\overline{L}$ implies that the condition for the neglect of the spatial derivative is

$$\overline{\Lambda}\ll\frac{1}{\sqrt{\overline{L}}}. \tag{41}$$

It can be seen from Eq. (40) that K' diverges as $\overline{\Lambda}\sqrt{\overline{L}}\to 0$ for T constant. We therefore define the mean-field limit as the limit where $\overline{\Lambda}\sqrt{\overline{L}}\to 0$ and $T\to 0$ in such a way that K' is finite. Note that by introducing a modified cooperation length defined as $l_c'=c/\omega_r\rho'$ it is possible to write the mean-field condition (41) as

$$\Lambda'=\frac{\Lambda}{l_c'}\ll 1,$$

and the damping constant K' as

$$K'=\frac{T}{\Lambda'},$$

so that K' can be interpreted as a scaled cavity mode linewidth.

In order to satisfy simultaneously Eq. (41) and the geometric restriction $\overline{\Lambda}>\overline{L}$, it is necessary that $\overline{L}\ll 1$, i.e., $L\ll l_c$ which is the usual type of condition quoted for validity of the mean-field approximation in that the sample must be optically thin with respect to some characteristic length (l_c in this case) . We have shown in Eq. (41), however, that there is also an upper limit to the cavity length for which the mean-field approximation is valid. This nonintuitive result is confirmed by a numerical solution of Eqs. (25)–(27) with the boundary condition (33) (Fig. 3). Figure 3(a) shows the spatial evolution of the field amplitude in the sample at a fixed time for cases where Eq. (41) is well satisfied. It can be seen that the fractional variation in the field amplitude across the sample is extremely small, around 3%, so that the mean-field approximation is clearly valid in this case. In Fig. 3(b) we show a case where Eq. (41) is no longer satisfied and it can be seen that the fractional variation in the field amplitude is no longer negligible, being around 250%, even though we still have $\overline{L}\ll 1$.

Recalling the fact that the width of the superradiant pulse in free space scales as $1/\sqrt{\overline{z}}$ allows us to propose a simple physical argument for the ring cavity mean-field limit (41). The scaled time duration of the pulse emitted from the sample will be $\Delta\overline{t}\sim 1/\sqrt{\overline{L}}$ so its spectral width will be $\Delta\overline{\omega}\sim\sqrt{\overline{L}}$. As the frequency spacing between cavity modes written in the same notation is $\Delta\overline{\omega}_{cav}\sim 1/\overline{\Lambda}$, the mean-field condition (41) is just the condition that the cavity mode spacing is much greater than the spectral width of the pulse, $\Delta\overline{\omega}_{cav}\gg\Delta\overline{\omega}$ ensuring that only a single cavity mode is excited.

Assuming the mean-field limit is satisfied we can rewrite the full set of coupled evolution equations for the atoms and field neglecting the spatial derivative and using $A'(\overline{t'})=\overline{A'}(\overline{t'})+A_I'/\sqrt{T}$, so that

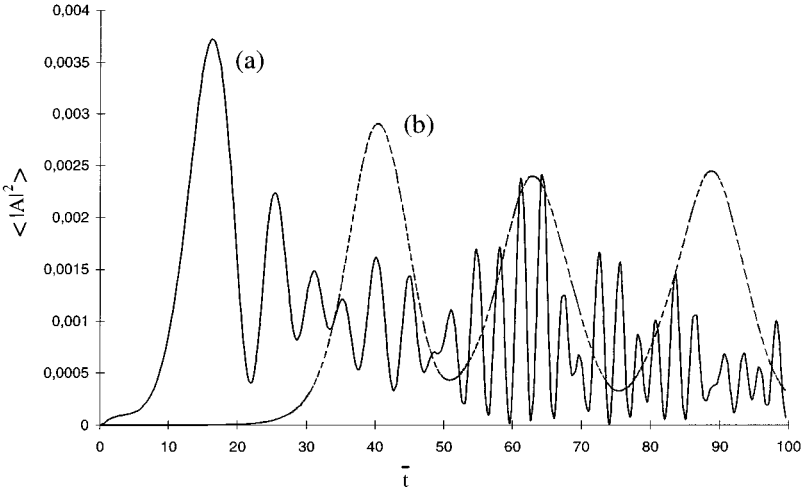

FIG. 4. Average scaled field intensity $\langle|A|^2\rangle$ as a function of $\bar{t}$ for (a) the bad cavity limit: $\bar{L}=0.0001$, $\bar{\Lambda}=0.01$, $T=0.02$, and $|A_I|=0.001$, i.e., $K'=9.3$. (b) the good cavity limit: $\bar{L}=0.01$, $\bar{\Lambda}=1$, $T=0.001$, and $|A_I|=0.001$, i.e., $K'=0.0046$.

$$\frac{d\theta_j}{d\bar{t}'}=p_j', \tag{42}$$

$$\frac{dp_j'}{d\bar{t}'}=-(A'e^{i\theta_j}+\text{c.c.}), \tag{43}$$

$$\frac{dA'}{d\bar{t}'}+K'\left(A'-\frac{A_I'}{\sqrt{T}}\right)=b. \tag{44}$$

The qualitative behavior of the system in the mean-field limit is therefore dependent only on the scaled damping parameter K'.

We now consider the limit of strong damping ($K'\geqslant 1$) and weak damping ($K'\ll 1$), where $A_I'/\sqrt{T}\ll 1$.

$K'\geqslant 1$: In the strong damping or ''bad cavity'' limit, we can adiabatically eliminate the field variable in Eq. (44) so that $A'\approx b/K'$. The scaled intensity $|A'|^2$ initially grows as $|A'|^2\propto e^{\bar{t}'/\sqrt{K'}}$. The radiated power in the strong damping limit, therefore, scales as

$$\epsilon_0|\bar{E}|^2=\hbar\omega n\rho\left(\frac{L}{\Lambda}\right)^{4/3}\frac{1}{K'^2}\propto n^2L^2 \tag{45}$$

and is independent of the cavity length. Note that this is only true while the mean-field condition (41) is satisfied. The fact that the radiated power $P\propto n^2$ indicates that superradiant behavior occurs in the bad cavity limit (see Fig. 4) similar to the case of a two-level system enclosed in a cavity [7]. The superradiant emission from the sample is, therefore, not sensitive to the presence of the cavity in this limit.

$K'\ll 1$: In the weak damping or ''good cavity'' limit, we can neglect the term containing K' in Eq. (44). The set of equations (42)–(44) now has no free parameters, and is identical to the set of Compton FEL equations in the steady-state limit [9], so the scaled intensity $|A'|^2$ grows as $|A'|^2\propto e^{\sqrt{3}\,\bar{t}}$ before saturating at a value of approximately 1.4 (see Fig. 4). This implies that the radiated power in the weak damping limit scales as

$$\epsilon_0|\bar{E}|^2=\hbar\omega n\rho\left(\frac{L}{\Lambda}\right)^{4/3}|A'|^2\propto\left(n\frac{L}{\Lambda}\right)^{4/3}. \tag{46}$$

The characteristic superradiant behavior ($P\propto n^2$) is therefore lost because of the narrow cavity linewidth.

Figure 4(a) shows the temporal evolution of the average field intensity in the atomic sample for a case where $K'>1$. The emission consists of a large amplitude pulse followed by a series of smaller pulses, similar to that observed in studies of superfluorescence in two-level systems [7]. Figure 4(b) shows the temporal evolution of the average field intensity in the atomic sample for cases where $K'\ll 1$. The intensity at the first saturation peak is $\approx 1.4(\bar{L}/\bar{\Lambda})^{4/3}=0.0028$ as predicted by Eq. (46) and the evolution is identical in form to that of the Compton FEL where propagation effects are neglected [9]. We emphasize that the probe saturation intensity is independent of the initial probe intensity which may result from noise. When the system starts from noise in the FEL it has been termed self-amplified spontaneous emission [9]. The scaled power output from the cavity is $T|A|^2\propto K'|A'|^2$. Figure 5 shows a plot of $K'|A'|^2$ against K' as calculated from the mean-field equations (42)–(44). The maximum value of $K'|A'|^2$ occurs when $K'\approx 1$. From the definition of K' (40), this means that the value of T which optimizes the power output from the cavity is $T\approx(\bar{\Lambda}\sqrt{\bar{L}})^{2/3}$.

V. DOPPLER BROADENING

A. General effects of Doppler broadening

Let us consider atoms with a Gaussian distribution of momenta. As the atoms all have different momenta they will debunch with time, even if they undergo no interaction with the probe field. We define τ_{db} as the characteristic time over which this Doppler debunching occurs and we evaluate it using the following argument.

The bunching factor b (16) may be written with averages in integral form

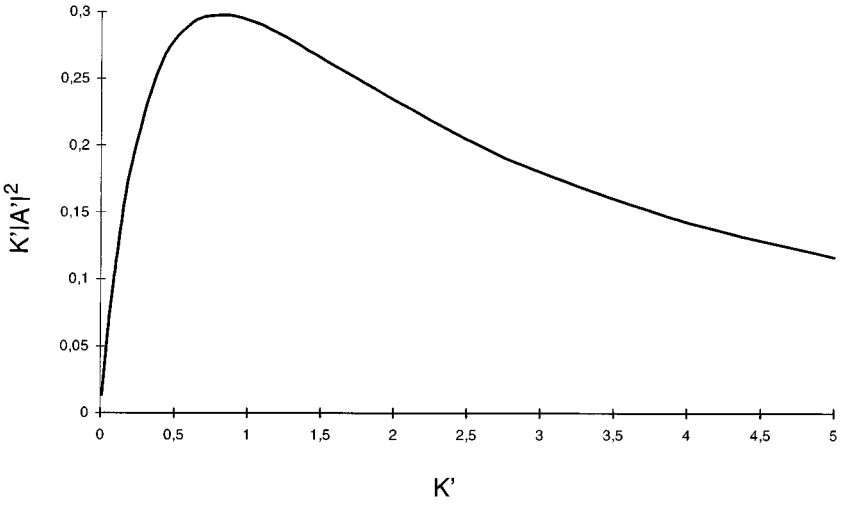

FIG. 5. $K'|A'|^2 \propto T|A'|^2$ (the scaled output power as a function of K').

$$b=\langle e^{-i\theta_j}\rangle_{\theta_0,\overline{p_0}}$$

$$=\frac{1}{2\pi}\int_0^{2\pi}d\theta_0\int_{-\infty}^{\infty}d\overline{p_0}G(\overline{p_0},\delta)e^{-i\theta(\overline{z},\overline{t};\theta_0,\overline{p_0})}, \quad (47)$$

where

$$G(\overline{p_0},\delta)=\frac{1}{\sqrt{2\pi}\overline{\sigma}}\exp-\left(\frac{(\overline{p_0}-\delta)^2}{2\overline{\sigma^2}}\right)$$

is a Gaussian momentum distribution function of width $\overline{\sigma}$ centred at $\overline{p_0}=\delta=(\omega_2-\omega_1)/(\omega_r\rho)$. As in Eq. (28) we have assumed that the mean initial atomic velocity is zero. The Doppler linewidth scaled with respect to the ''collective linewidth'' $\omega_r\rho$ is

$$\overline{\sigma}=\frac{k\Delta v}{\omega_r\rho},$$

where Δv is the velocity spread of the atomic beam. In the limit of weak interaction, i.e., $|A|\ll 1$, the atomic phases $\theta_j\approx\theta_{0j}+\overline{p_{0j}}\,\overline{t}$, so that from Eq. (47)

$$|b|\propto\exp\left(-\frac{\overline{\sigma^2}\,\overline{t^2}}{2}\right). \quad (48)$$

The effect of Doppler broadening is, therefore, to cause the bunching to decay with a characteristic decay time of

$$\tau_{db}=\frac{1}{\overline{\sigma}} \quad (49)$$

Defining τ_g as the growth time of b in the cold beam limit, then if $\tau_{db}\ll\tau_g$ we expect the evolution of the bunching and, consequently, the field to be restricted severely by the atomic Doppler debunching due to the spread in atomic momenta. Conversely, if $\tau_{db}\gg\tau_g$, the growth of the bunching and field is expected to be restricted only slightly by the Doppler debunching. In Sec. V B this simple argument is investigated for the case of superradiant field evolution.

B. The effect of Doppler broadening on superradiance

We consider the case of CARL evolution in a ring cavity, which is described by Eqs. (42)–(44). As shown in Sec. IV, it is useful to normalize variables with respect to ρ'. We must therefore define

$$\overline{\sigma'}=\frac{k\Delta v}{\omega_r\rho'}=\overline{\sigma}\left(\frac{\Lambda}{L}\right)^{1/3}, \quad (50)$$

$$\delta'=\frac{\omega_2-\omega_1}{\omega_r\rho'}=\delta\left(\frac{\Lambda}{L}\right)^{1/3}, \quad (51)$$

and $\tau'_{db}=1/\overline{\sigma'}$. We consider specifically the case of a ''bad'' cavity, where $K'\geqslant 1$. When $\overline{t'}\gg 1/K'$, it is possible to eliminate the field variable A' adiabatically, so that

$$A'\approx\frac{A'_I}{\sqrt{T}}+\frac{b}{K'}.$$

When $b/K'\gg A_I/\sqrt{T}$ then $A'\propto b$, which when combined with Eq. (48) suggests that the scaled probe intensity $|A'|^2$ will have a Gaussian dependence on $\overline{\sigma'}$.

In Fig. 6 we plot the scaled intensity $|A'|^2$ as a function of $\overline{t'}$ for three different values of $\overline{\sigma'}$, as calculated form a numerical solution of Eqs. (42)–(44). The effect of the momenta spread is clearly to reduce the peak intensity of the pulse ($|A'_p|^2$).

A plot of the peak intensity $|A'_p|^2$ against $\overline{\sigma'^2}$ as calculated from a numerical solution of Eqs. (42)–(44) is shown in Fig. 7 for the case where $K'=8$. It shows that when $|A'|\gg|A_0|$ the dependence of $|A'_p|^2$ on $\overline{\sigma'}$ is well described by a Gaussian function, i.e., $|A'_p|^2\propto\exp(-\overline{\sigma'^2}/\beta^2)$, where β is the width of the Gaussian. This is not true when $A'\sim A_0$ because in this case A' is no longer proportional to b.

By repeating these calculations for different values of K' and calculating the gradient of the $\ln|A'_p|^2$ against $\overline{\sigma'^2}$ curve, we can show that β varies as $\sqrt{K'}$ (Fig. 8). The dependence of $|A'_p|^2$ on $\overline{\sigma'}$ can then be approximated by a Gaussian function of the form

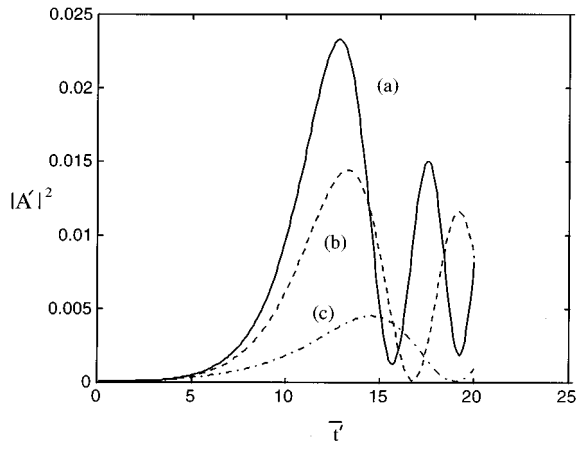

FIG. 6. Scaled radiation power $|A'|^2$ as a function of $\overline{t'}$, when $\delta'=0$ and $K'=8$ for the scaled atomic momenta spreads (a) $\overline{\sigma'}=0$, (b) $\overline{\sigma'}=0.1$, and (c) $\overline{\sigma'}=0.2$.

$$|A_p|^2 \propto \exp(-\alpha \overline{\sigma'}^2 K'), \tag{52}$$

when $|b|/K' \gg |A_I|/\sqrt{T}$, where α is a numerical factor. From the results of Sec. III, the characteristic growth time of the field for a bad ring cavity is

$$\tau'_g = \tau'_{sr} = \sqrt{K'}, \tag{53}$$

so Eqs. (52) and (53) confirm that when $\tau'_{db} \gg \tau'_{sr}$ ($\overline{\sigma'} \ll 1/\sqrt{K'}$) the spread in atomic momenta has little effect on the peak intensity of the probe field. This is, therefore, the ''cold beam limit'' for CARL in a bad ring cavity. In contrast, when $\tau'_{db} < \tau'_{sr}$ the peak intensity of the probe field is greatly reduced by the spread in atomic momenta. The second limit will be considered in more detail in the following sections.

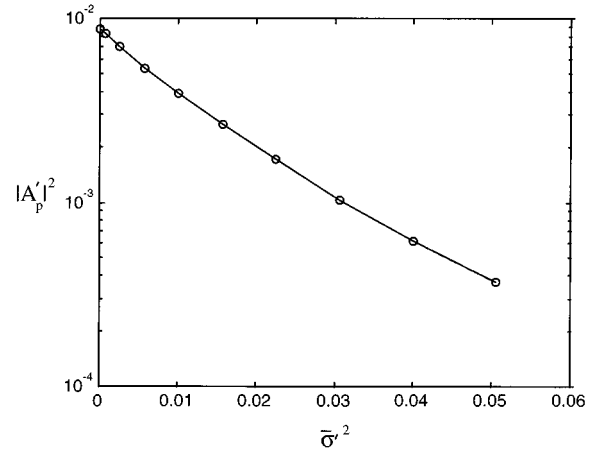

FIG. 7. Scaled peak radiaton power $|A'_p|^2$ as a function of the square of the scaled atomic momenta spread $\overline{\sigma'}^2$ for a bad ring cavity ($K'=8$), when $\delta=0$ and $A_0=0.01$.

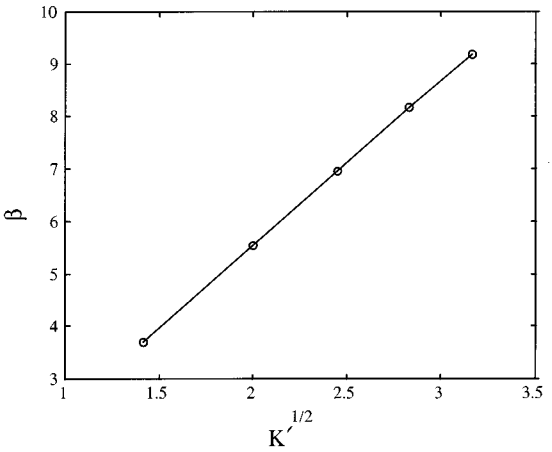

FIG. 8. Gradient of $\ln|A'_p|^2$ vs $\overline{\sigma'}^2$ curve of Fig. 7 as a function of K'.

C. Noncollective gain

In this section we consider the case of a bad cavity where the debunching time τ'_{db} is less than τ'_{sr}, so that the momentum spread has a significant effect on the field evolution. We investigate CARL in a bad ring cavity, which is described by Eqs. (42)–(44) with $K' \geqslant 1$, so $A' \approx A_0 + b/K'$, where $A_0 = A'_I/\sqrt{T}$. If we assume $b/K' \ll A_0$, then we can replace A' by A_0 in the atomic motion equation (43) so that

$$\frac{d\overline{p'_j}}{d\overline{t'}} = -(A_0 e^{i\theta_j} + \text{c.c.}),$$

i.e., the atoms are assumed to evolve under the action of the input field only, and the atomic phases evolve as

$$\theta_j \approx \theta_{0j} + \overline{p'_{0j}}\,\overline{t'}.$$

Under these assumptions, the gain of the probe field, defined as $\mathcal{G} = (|A'|^2/|A_0|^2) - 1$, behaves as [11]

$$\mathcal{G}(\delta') \propto \left.\frac{\partial G}{\partial \overline{p'_0}}\right|_{\overline{p'_0}=0}, \tag{54}$$

when $\overline{t'} \gg \tau'_{db}$, where $G(\overline{p'_0}, \delta')$ is the momentum distribution function defined earlier. The behavior of the gain as a function of $\overline{t'}$ is shown in Fig. 9 as calculated from Eqs. (42)–(44) for different values of δ'. Notice that the gain is significantly smaller than that for the cold beam evolution by approximately six orders of magnitude (see Fig. 4). Figure 10 shows a graph of $\mathcal{G}$ against δ'. These points are a good fit to the curve which is the derivative of a Gaussian. Maximum amplification of the probe occurs when $\delta' = \overline{\sigma'}$ and maximum absorption of the probe occurs when $\delta' = -\overline{\sigma'}$.

The physical mechanism behind this type of gain has been described quantum mechanically in terms of stimulated Raman scattering so we will refer to it, henceforth, as Raman gain [2]. We describe it here classically in terms of a process analogous to Landau damping of a wave by electrons or ions in a plasma [12]. The ponderomotive potential produced by the combination of the pump and probe fields has a phase

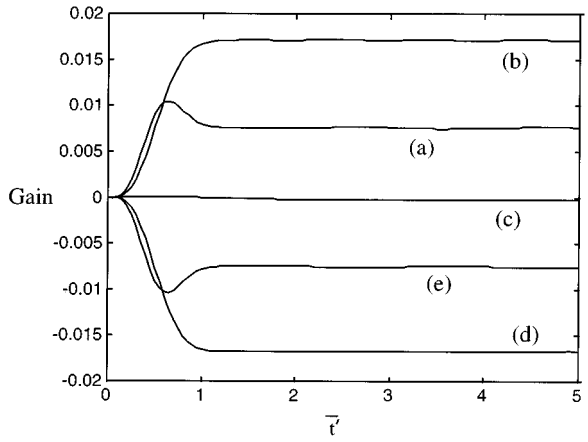

FIG. 9. Radiation power gain as a function of $\bar{t}'$ for a bad cavity ($K'=10$) and warm beam ($\bar{\sigma}'=3$) for the detuning parameters: (a) $\delta'=6$, (b) $\delta'=3$, (c) $\delta'=0$, (d) $\delta'=-3$, and (e) $\delta'=-6$.

velocity v_{ph} given by Eq. (23). This means that atoms with initial momenta $\bar{p}_0'$ slightly less than zero ($v<v_{ph}$) will be accelerated and those with $\bar{p}_0'$ slightly more than zero ($v>v_{ph}$) will be decelerated due to the force exerted by this potential. As the atomic momenta are nonuniformly distributed, the number of atoms accelerated and the number decelerated will not be equal in general, so there will be a net exchange of energy with the probe field. The amount of energy exchanged will be proportional to the difference in momentum group population around $\bar{p}_0'=0$, i.e., $\partial G/\partial \bar{p}_0'$ at $\bar{p}'=0$ (Fig. 11). Note that this gain mechanism is not collective as only the pump field A_0, which is independent of b, drives the atomic motion. The atoms, therefore, evolve independently of one another behaving as decoupled pendula. This noncollective gain mechanism explains qualitatively the experimental results of Courtois *et al. [2] involving a small sample of cesium atoms in free space, where no cavity is present. The explanation given above is also relevant for experiments involving no cavity. When the atomic sample is very short with respect to the cooperation length, i.e.,* $\bar{L}\ll 1$*, the field distribution across the sample is almost uniform. Propagation effects can then be approximated by using a damping term to model the effect of radiation loss in the atomic sample due to propagation [11]. The equations describing CARL in free space (25)–(27) therefore, reduce to a set similar to Eqs. (42)–(44)*

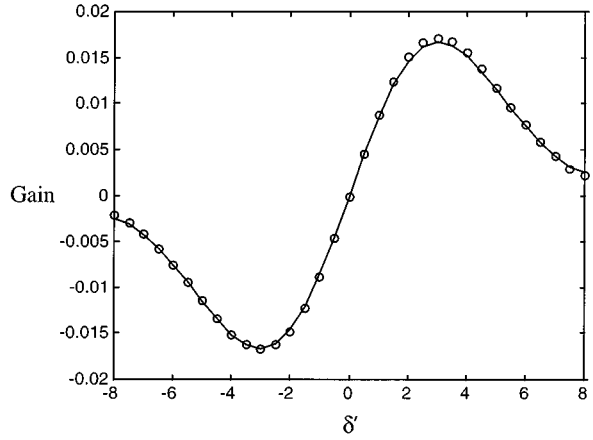

FIG. 10. Radiation power gain as a function of detuning δ' for parameters $K'=10$ and $\sigma'=3$. A (solid) Raman gain curve, which is the derivative of the Gaussian atomic momenta distribution function, is fitted to the points from numerical simulations.

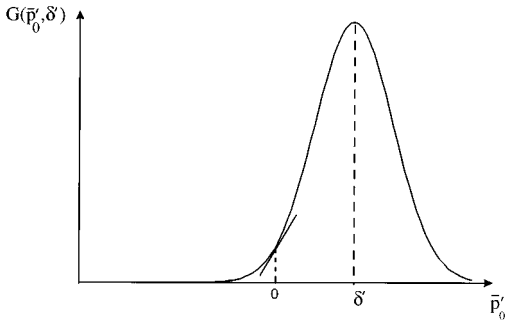

FIG. 11. Schematic diagram showing how the Raman gain mechanism depends upon the atomic detuning δ'.

$$\frac{d\theta_j}{d\bar{t}}=p_j, \tag{55}$$

$$\frac{d\bar{p}_j}{d\bar{t}}=-(Ae^{i\theta_j}+\text{c.c.}), \tag{56}$$

$$\frac{dA}{d\bar{t}}+K_f(A-A_I)=b, \tag{57}$$

where the free space damping constant $K_f=1/\bar{L}$, which is assumed to be much larger than one, so that $A\approx A_I$. The results described above for a ring cavity, therefore, also apply to a short atomic sample in free space. This is confirmed by a comparison of Fig. 9, showing bad cavity, warm beam evolution, with Fig. 12, which shows a graph of the intensity

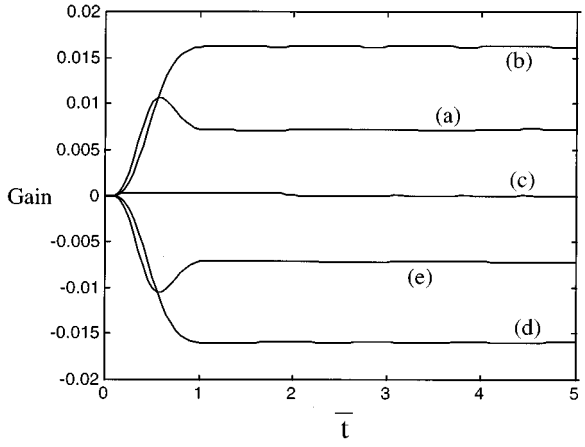

FIG. 12. Radiation power gain as a function of $\bar{t}$ for free space evolution, when $\bar{\sigma}=3$, $\bar{L}=0.1$ and (a) $\delta=6$, (b) $\delta=3$, (c) $\delta=0$, (d) $\delta=-3$, and (e) $\delta=-6$.

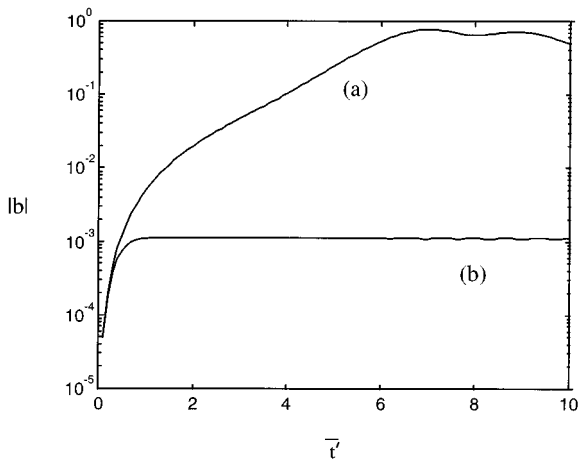

FIG. 13. Bunching parameter $|b|$ as a function of $\overline{t'}$ for cold (solid line) and warm (dashed line) beams. These correspond to Figs. 4(a) and 9(b), respectively.

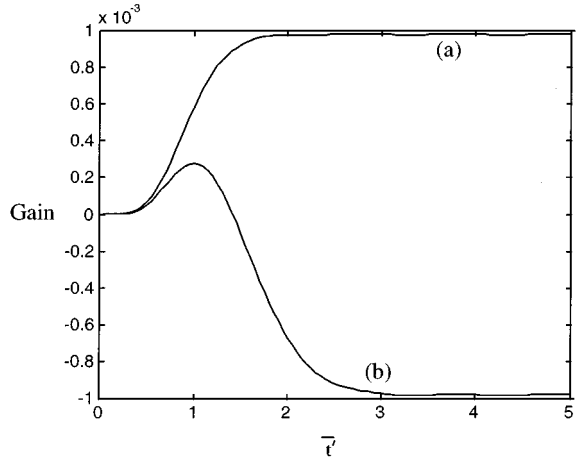

FIG. 14. Radiation power gain as a function of $\overline{t'}$ for parameters $\overline{\sigma'}=2$, $K'=8$, and $\delta=0$, and for (a) $A'=A_0$ in Eq. (43) — i.e., no probe field evolution and (b) $A'=A_0+b/K'$ in equation (43) — i.e., including probe field evolution.

($|A|^2$) evolution as a function of $\overline{t}$ for a warm beam at the sample end ($\overline{z}=\overline{L}$), as calculated from a numerical solution of the free space evolution equations including propagation (25)–(27) for different values of δ. In what follows, it is understood that the results derived for a bad ring cavity can also be applied to a small atomic sample in free space by replacing $\overline{t'}$ with $\overline{t}$, A' with A, K' with K_f, $A_I'/\sqrt{T}$ with A_I, δ' with δ, and $\overline{\sigma'}$ with $\overline{\sigma}$. Hence, one can use a simple single-mode mean-field model as opposed to the more complex system describing propagation in full.

We are now in a position to compare the cold and warm beam limits. The large difference in gain, by approximately six orders of magnitude, can be seen from a comparison between the gains of the cold beam in Fig. 4 and the warm beam in Fig. 9.

For completeness we compare the bunching factors for the same cold and warm beams in Figs. 13(a) and 13(b), respectively. The maximum of the cold beam bunching factor of ≈ 0.8 is significantly larger than that of the warm beam value of 10^{-3}. Hence, we conclude that for warm beams, where Raman gain dominates, there is only a weak modulation of the atomic density. This is in dramatic contrast to the strong bunching obtained for cold beam evolution.

D. Competition between collective and noncollective effects

As in Sec. V C, we assume that we have a bad ring cavity and that debunching effects are strong ($\tau_{db}'<\tau_{sr}'$). We now consider the case where $\delta'=0$, i.e., $\partial G/\partial \overline{p_0'}|_{\overline{p_0'}=0}=0$. The analysis of [11], where the atoms evolve under A_0 only, predicts a nonzero but very small gain, with a temporal behavior, as shown in Fig. 14(a). A numerical solution of Eqs. (42)–(44) with the same parameters also gives a small gain, but with a different sign and a quite different temporal behavior, as shown in Fig. 14(b). The reason for this lies in the neglect of the reaction of the field emitted by the atoms (b/K') in the analysis of [11]. The negative gain in Fig. 14(b) can be deduced from the following argument: If the self-consistent field generated by the bunching (b/K') is included in the motion equation (43), then the total probe field $A'=|A'|e^{i\xi}=A_I/\sqrt{T}+b/K'$ is also a function of time. Therefore, as the field phase ξ is time varying, there will be a dynamic shift of the effective frequency of the probe field from

$$\omega_1 \rightarrow \omega_1 - \frac{\partial \xi}{\partial t}$$

and the effective phase velocity of the ponderomotive potential is shifted from

$$v_{ph} \rightarrow v_{ph} - \frac{1}{2k}\frac{\partial \xi}{\partial t}.$$

It can be shown that the sign of $d\xi/dt$ is positive [11], so the atomic sample acts as a dielectric medium with a refractive index greater than 1, which reduces the phase velocity of the ponderomotive potential. If this is taken into account, the resonant group of atoms are no longer those with $\overline{p_0'}=0$, but those with $\overline{p_0'}=d\xi/d\overline{t'}>0$. As $\partial G/\partial \overline{p_0'}<0$ at this point, i.e., for the group of atoms with velocity $v \approx v_{ph}-(1/2k)\partial\xi/\partial t$ there are more atoms traveling slightly slower than the ponderomotive potential than traveling slightly faster, the Raman gain mechanism described in Sec. V C takes effect, causing the atoms to absorb the probe after initially amplifying it. The dynamic frequency shift which produces the transient amplification of the probe is characteristic of collective behavior [9], as opposed to the Raman gain mechanism which is not collective in nature. As we are considering cases where debunching effects are strong, i.e., $\tau_{db}'<\tau_g'$, collective effects are very weak and are dominated by the Raman gain except when $\partial G/\partial \overline{p_0'}\approx 0$, i.e., when $\delta'\approx 0$ for a Gaussian momentum distribution. Some possible experimental evidence of such transient amplification has been recently observed by Verkerk [3].

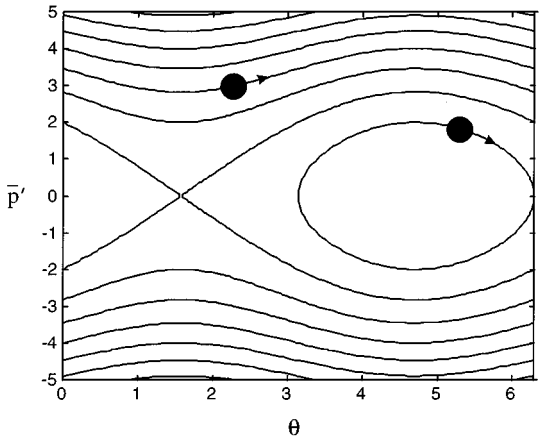

FIG. 15. Phase-space trajectories for atoms interacting with a constant field $A'=A_0=1$.

E. Long time scale synchrotron oscillations

An additional effect, which is nonlinear in nature and can occur after long interaction times, is that of the trapping of atoms by the ponderomotive potential. Let us again assume that debunching effects are strong and the gain of the probe field is small enough so that $A' \approx A_0 = A_I'/\sqrt{T}$.

From Eqs. (42) and (43), a phase trajectory for each electron can be constructed (Fig. 15). This is identical to the phase trajectory for a simple pendulum. The particles which have values of $\overline{p_0'}$ that lie inside the separatrix are trapped in potential wells and will eventually execute oscillations about the bottom of the well. The period of these oscillations can be estimated from an inspection of the atomic motion equations (42) and (43) which when combined can be written as

$$\frac{d^2\theta_j}{d\,\overline{t'}^2} + 2|A_0|\cos(\theta_j + \xi_0) = 0,$$

where $A_0 = |A_0|e^{i\xi_0}$. The atoms close to the bottom of the potential will therefore oscillate with angular frequency $\omega_s \approx \sqrt{2|A_0|}$. The period of the oscillations is, therefore,

$$\tau_s' = \frac{2\pi}{\omega_s} = \pi\left(\frac{2}{|A_0|}\right)^{1/2}.$$

In the analysis of [11], the perturbation of the atomic phase due to the ponderomotive potential is assumed to be negligible in Eq. (43) and the probe gain attains a steady state for times $\overline{t'} \gg \tau_{db}'$. This assumption is only valid for time $\overline{t'} \ll \tau_s'$. For $\overline{t'} \sim \tau_s'$, the trapping of some of the atoms in the potential causes the steady state to become unstable and these atoms oscillate, analogous to the synchrotron oscillations of electrons in the FEL, causing the field to depart from the steady state. Confirmation of this is shown in Fig. 16, which shows the evolution of the probe gain when $\overline{t'} \ll \tau_s'$ [graph (a)] and the equivalent case when $\overline{t'} \sim \tau_s'$ [graph (b)] calculated from Eqs. (42)–(44). Note that in order to observe any region of steady-state gain, it is necessary that $\tau_s' > \tau_{db}'$, i.e., $|A_0| < 2\pi^2\overline{\sigma'}^2$. This particle trapping mechanism is one possible explanation for some experimental results observed by Verkerk [3], which show the probe gain growing initially to a steady state before decreasing. The further revival and oscillation of the gain have yet to be observed.

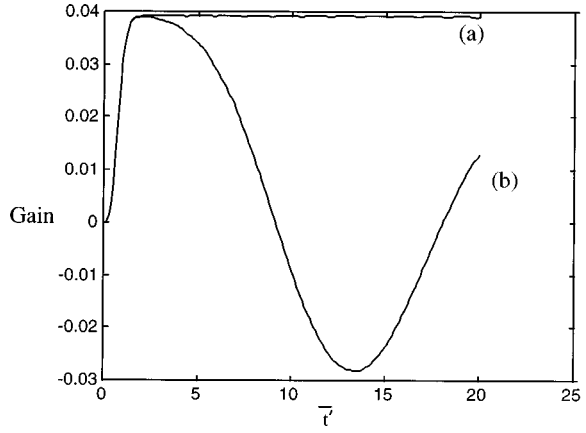

FIG. 16. Radiation gain as a function of $\overline{t'}$ for parameters $\overline{\sigma'}=2$, $\delta'=2$, and (a) $|A_0|=0.001$ ($\tau_b'=112$)— no particle trapping and (b) $|A_0|=0.1$ ($\tau_b'=11.2$) — particle trapping leading to synchrotron instability.

VI. RADIATION PRESSURE EFFECTS

In the mean-field limit radiation pressure is modeled by adding the radiation pressure term $\Gamma' = -\Omega^2\gamma/[2(\Delta^2 + \Omega^2)\omega_r\rho'^2]$ to Eq. (43) analogous to Eq. (21). (As previously noted in Sec. V C both free space and mean-field limit evolution are similar for $K \geqslant 1$ and $K' \geqslant 1$, so that the following analysis also holds for free space, short pulse evolution.)

We first consider the cold beam limit $\overline{\sigma'}=0$ with $K'=5$ and the atoms initially detuned for maximum gain in the absence of radiation pressure $\delta'=0$, for three different values of Γ'. The results of the numerical integration are shown in Fig. 17. Figure 17(a) shows the case for $\Gamma'=0$ and

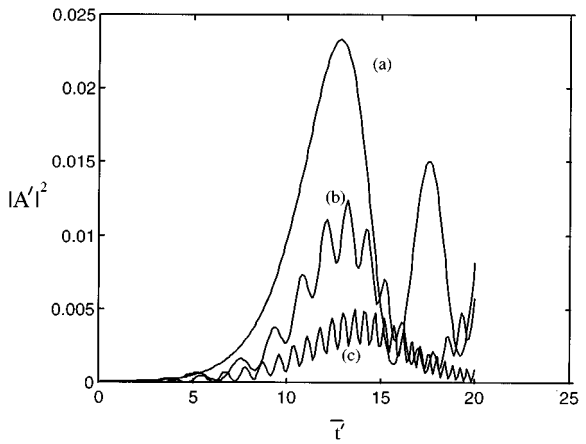

FIG. 17. Effects of radiation pressure on a cold beam in the mean-field limit with: $K'=5$, $\overline{\sigma'}=0$, $\delta'=0$, and (a) $\Gamma=0$, (b) $\Gamma=0.4$, and (c) $\Gamma=0.8$.

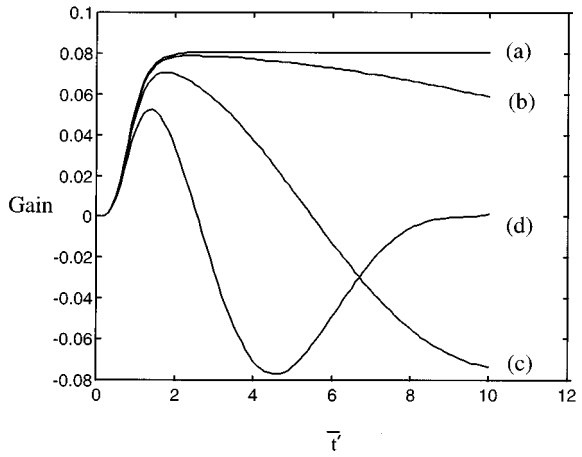

FIG. 18. Effects of radiation pressure on a warm beam in the mean-field limit with: $K'=5$, $\overline{\sigma'}=2$, and $\delta'=2$ and (a) $\Gamma=0$, (b) $\Gamma=0.1$, (c) $\Gamma=0.4$, and (d) $\Gamma=1$.

corresponds to the solution without radiation pressure shown in Fig. 6(a). On increasing Γ' two effects are noticeable. The first is that the peak intensity of the radiation emitted is reduced. This effect may be accounted for by recognizing that the atoms will be ''swept'' out of resonance by the radiation pressure so that they will no longer be detuned for maximum gain to occur. In fact, the further they are swept from resonance the smaller will be the gain of the probe. The second effect is the modulation of the probe radiation's wave envelope. The modulation frequency increases approximately linearly in t' indicating a frequency chirp of the emitted radiation. The frequency of the radiation emitted by the atoms as a function of t' approximately corresponds to their instantaneous resonant frequency. The instantaneous period of the probe field modulation may be simply calculated: The effective detuning of the atoms at time t' due to the radiation pressure term Γ' will be $\delta'_{\rm eff}=\Gamma' t'$. The instantaneous modulation period $\Delta t'$ will then be given by $\Delta t'=2\pi/\delta'_{\rm eff}$. This simple analysis gives good agreement with the graphs of numerical simulations of Figs. 17(a) and 17(b).

In the warm beam limit an instability of the steady-state Raman gain can be induced by the effect of radiation pressure. A typical result of a numerical solution to the equations is shown in Fig. 18 where we plot the gain for different values of the radiation pressure term Γ'. The steady-state evolution becomes unstable as the radiation pressure term Γ' is increased from zero. In particular, for smaller values of Γ' one observes a monotonic decrease in gain similar to the experimental observations of Ref. [5]. As Γ' is increased the gain saturates, decreases to a negative minimum, and then approaches zero asymptotically. We stress that in this case synchrotron oscillations do not occur, i.e., the gain does not become positive again, as in Fig. 16(b), as radiation pressure and particle trapping effects arise from completely different mechanisms. The transient behavior of Fig. 18 can be interpreted by reference to the Raman gain curve of Fig. 10. The radiation pressure has the effect of decreasing the atomic momenta and so their effective detuning with respect to the Raman gain curve. The atoms then traverse the gain curve and are swept from maximum gain, at $\delta'=\overline{\sigma'}$, through zero and into the region of negative gain before tending to zero. To date only the region of monotonic decrease of the gain has been observed experimentally, the minimum and subsequent approach to zero gain have not.

VII. CONCLUSIONS

A semiclassical model of CARL has been derived and was used to investigate propagation, cavity, and Doppler-broadening effects. The effects of propagation were investigated for cases where the atomic sample is in free space and enclosed in a ring cavity. In free space, it was found that a superradiant solitonlike pulse of radiation was produced. In a ring cavity, the condition for the neglect of propagation effects was found to be $\overline{\Lambda}\sqrt{\overline{L}}\ll 1$. When this mean-field condition is satisfied, the dynamics of CARL interaction in a ring cavity is described by a damping parameter, $K'=T/(\overline{\Lambda}\sqrt{\overline{L}})^{2/3}$. When $K'\ll 1$, the cavity is said to be ''good,'' and the field evolution is identical to that in a Compton FEL neglecting slippage. When $K'\geqslant 1$, the cavity is said to be ''bad,'' and a super-radiant pulse of radiation is produced. The effect of Doppler broadening on CARL evolution was shown to be a reduction in bunching due to the spread in atomic momenta. For the case of atomic samples in a bad cavity it was shown that the effect of Doppler broadening on the maximum probe field intensity can be deduced from a comparison of the debunching time τ'_{db} with the growth time of the bunching and field τ'_{sr} neglecting Doppler broadening. When $\tau'_{db}\gg\tau'_{sr}$, the evolution of the field is essentially unaffected by Doppler broadening, so this condition is the ''cold beam limit.'' If $\tau'_{db}<\tau'_{sr}$, however, the field evolution is greatly restricted by Doppler broadening. Under these conditions, collective growth of the field is very weak and can be dominated by noncollective effects such as Raman gain due to the shape of the momentum distribution. However, due to trapping of atoms in the ponderomotive potential, synchrotron type oscillations will eventually drive the probe field for sufficiently long interaction times. The results described here should help to clarify the distinction between true CARL behavior and the noncollective phenomena which occur due to recoil in systems of strongly driven atoms such as Raman scattering. True CARL behavior exhibits strong bunching, or modulation, of the atoms, while in noncollective behavior only a weak bunching is obtained. In the cold beam limit the effects of radiation pressure were to reduce the peak intensity the emitted radiation and also to introduce a frequency chirp onto it. Both results were described in terms of the linearly decreasing effective detuning of the atoms. In the warm beam limit, the effect of radiation pressure is to force a departure of the probe gain from its steady-state value. This effect has been explained in terms of a sweeping of the atomic detuning through the Raman gain spectrum. The modulation of the field intensity envelope was not observable as the spread in the atomic momenta means that there is a spread of resonant frequencies, so that a simple sinusoidal type modulation will not occur.

ACKNOWLEDGMENTS

The authors would like to thank the Royal Society of London and the EPSRC for support of G.R.M.R. and B.McN., respectively.

[1] R. Bonifacio and L. De Salvo, Nucl. Instrum. Methods Phys. Res., Sect. A **341**, 360 (1994); R. Bonifacio, L. De Salvo, L. M. Narducci, and E. J. D'Angelo, Phys. Rev. A **50**, 1716 (1994).
[2] J. Y. Courtois, G. Grynberg, B. Lounis, and P. Verkerk, Phys. Rev. Lett. **72**, 3017 (1994).
[3] P. Verkerk, in *Coherent and Collective Interactions of Particles and Radiation Beams*, Proceedings of the International Course of Physics ''Enrico Fermi,'' Course CXXXI, edited by A. Aspect, W. Barletta, and R. Bonifacio (IOS Press, Amsterdam, 1996), p. 325.
[4] P. R. Hemmer *et al.*, Phys. Rev. Lett. **77**, 1468 (1996).
[5] S. Guibal *et al.*, Opt. Commun. **131**, 61 (1996).
[6] F. T. Arecchi and R. Bonifacio, IEEE J. Quantum Electron. **1**, 169 (1965).
[7] L. Allen and J. H. Eberly, *Optical Resonance and Two Level Atoms* (Dover, New York, 1987).
[8] R. Bonifacio and L. De Salvo, Opt. Commun. **115**, 505 (1995).
[9] R. Bonifacio, F. Casagrande, G. Cerchioni, L. De Salvo, P. Pierini, and N. Piovella, Riv. Nuovo Cimento **13**, 9 (1990), and references therein.
[10] N. Piovella, Opt. Commun. **83**, 92 (1991).
[11] R. Bonifacio and P. Verkerk, Opt. Commun. **124**, 469 (1996).
[12] F. F. Chen, *Introduction to Plasma Physics and Controlled Fusion* (Plenum, London, 1984).